Intermetallics 154 (2023) 107823

Contents lists available at ScienceDirect

Intermetallics

journal homepage: www.elsevier.com/locate/intermet

Structural transitions and magnetocaloric properties of low-cost MnNiSi-based intermetallics

B.G.F. Eggert [a], J.F.H. Belo [b], J.P. Araújo [b], B.C. Hauback [a], C. Frommen [a,*]

[a] Department for Hydrogen Technology, Institute for Energy Technology (IFE), P.O. Box 40, NO-2027, Kjeller, Norway
[b] Institute of Physics of Advanced Materials, Nanotechnology and Nanophotonics (IFIMUP), Departamento de Física e Astronomia da Faculdade de Ciências da Universidade do Porto, Rua do Campo Alegre, 687, 4169-007, Porto, Portugal

ARTICLE INFO

Keywords:
A. intermetallics
Functional alloys
B. Matertensitic transformation
Magnetic properties
D. microstructure
F. Electron microscopy
Scanning

ABSTRACT

A series of $Mn_{1-x}Ni_{1-x}Fe_{2x}Si_{0.95}Al_{0.05}$ MM'X-type compounds (with x = 0.28, 0.3, 0.32 and 0.35) were investigated for their potential as magnetocaloric materials. Structural and magnetic properties were studied by magnetometry, microscopy and X-ray diffraction. Double substitution of Fe in Mn and Ni sites allowed to tune martensitic transition temperatures between low temperature orthorhombic and high temperature hexagonal structures from 373 K in x = 0.28–183 K in x = 0.35 during cooling. Transition temperatures occur around room temperature for x = 0.30 (300 K for cooling transformation) and 0.32 (270 for heating transformation). Isothermal entropy changes of −8, −19 and −26 J/kg.K were calculated for field changes of $\mu_0 H$ = 0–2, 0–5 and 0–7 T for x = 0.30. The values are comparable to those reported for MnNi(SiAl)-based compounds with single site substitutions (Mn and Ni) by Fe. Further analyses show that high magnetic fields are necessary to induce the magnetostructural transition in all studied compounds, which can be attributed to the presence of secondary phases and/or disorder at a local level.

1. Introduction

Materials featuring magnetoresponsive effects can be employed in a variety of applications. As an example, magnetostriction effects occur when magnetic fields modify internal strain in the crystal structure, giving rise to core components of transducers and actuators [1]. For magnetoresistance effects, the electrical resistance is modified by varying degrees of magnetic fields, which enables devices such as microelectromechanical systems and spin-valves [2,3]. Besides changes in strain and electrical resistivity, the reorientation of magnetic moments also brings a modification in temperature. In some materials, known as magnetocaloric materials, external magnetic fields induce a large variation in temperature compared to regular materials [4]. In some magnetocaloric materials, these large variations are created due to coupled magnetization and volume changes, undergoing transitions known as First Order Phase Transitions (FOPTs).

Such magnetocaloric phase transitions can be achieved by composition tuning of known systems, enabling concurrent electronic [5–8] and structural changes [9–11] in relation to magnetic transitions. In magnetocaloric materials with FOPTs, the latent heat associated with symmetry and/or volume changes around the coupled structural transition temperature T_{str} is the driving force for alternative energy conversion technologies. In order to evaluate the performance of such magnetocaloric materials, two properties are commonly considered: the adiabatic temperature change (ΔT_{ad}) and the isothermal entropy change (ΔS_m) [4,12]. If one considers the use of such materials for wide spread technologies such as domestic refrigeration and air conditioning, masses in the order of kilograms of magnetocaloric materials will be needed in each unit [13,14]. Therefore, magnetocaloric materials should be produced with non-expensive, non-critical elements, i.e., elements that are not at a supply risk, that do not feature major environmental implications in its production, and that do not feature a large vulnerability to supply restriction [15]. Such materials should also be inserted within a sustainable life cycle [14].

One of the most interesting and versatile class of materials which exhibit magnetoresponsive effects are the MM'X compounds, where M and M′ are transition metals, and X is a p-block element. Typical examples include MnCoGe, MnCoSi, MnNiGe among others [16]. These materials crystallize either in the orthorhombic (orth.) *TiNiSi* structure-type (space group *Pnma*) or the hexagonal Ni_2In structure-type (space group $P6_3/mmc$) at higher temperatures, as schematically illustrated for MnNiSi 2 × 2 × 2 supercells in Fig. 1. To ease comprehension,

* Corresponding author.
E-mail address: Christoph.frommen@ife.no (C. Frommen).

https://doi.org/10.1016/j.intermet.2023.107823
Received 12 October 2022; Received in revised form 20 December 2022; Accepted 2 January 2023
Available online 13 January 2023

TiNiSi and the Ni_2In structures will be referred to as orth. and hex. respectively. The *TiNiSi* structure-type is a ternary silicide with 3 different *4c* positions, with half-chair configuration in Ni–Si bonds. Ni and Si are also bonded to Mn, which itself is arranged with other Mn atoms in spiral/hexagonal coordination, if seen along the *b* direction. This spiral/hexagonal coordination is emphasized in Fig. 1a. It is known to be responsible for a high magnetic moment in this structure [17,18]. In the hex. Ni_2In type structure illustrated in Fig. 1b, the Mn atoms stay in layered positions along vertices and edges of the unit-cell (2*a* site), with Ni and Si remaining in 2*d* and 2*c* sites, respectively [19]. The orth. and hex. unit cells are related in the following manner: $c_{hex} \rightarrow a_{orth}$, $\sqrt{3}\, a_{hex} \rightarrow c_{orth}$, and $c_{hex} \rightarrow a_{orth}$. By appropriate elemental substitution, a magnetostructural transition (MST) can be achieved in MM'X systems across a wide compositional space [1,20–22]. Given a sufficiently high magnetic field, a metamagnetic transition can occur from a hex. paramagnetic (PM) to an orth. ferromagnetic phase (FM) [19].

Among the commonly studied MnMX compounds, MnNiSi features the more abundant Si element as a p-block, compared to critical Ge, regularly used in MM'X reports. The use of Ge as a main element in magnetocaloric devices would require a much larger demand than the possible future production, making its use inviable [14]. Also, the price of Ge is much larger than Si. Therefore, MnNiSi should be used as a starting MM'X compound. Its structural transition temperature (T_{str}) is close to 1200 K, while its T_C is around 600 K [19], and different elements can partially substitute the 2*a*, 2*d*, or 2*c* sites according to the Hume-Rothery rules (referring to the hex. structure). In some compounds, it is possible to completely substitute one element for another while remaining in the same space groups, yielding different forms of magnetism i.e. antiferromagnetism in MnNiGe [19], paramagnetism in FeNiSi [23] or ferromagnetism in MnCoGe and MnNiSi [17,24]). This is another indication of the versatility of this class of materials. In the case of MnNiSi, at least two substitutions in the lattice must be performed to induce an MST around room temperature (RT); one on either the 2*a* or 2*d* sites, and a second on the 2*c* sites (when referring to the Ni_2In structure type).

2*d* and 2*a* site substitutions in MM'X systems are usually performed by other transition metals, where the T_{str} modifications are site and content dependent [25]. With regards to the effect of substitution in 2*c* sites, different p-block elements can be used, mainly from groups 3a and 4a i.e. Ge [26–28], Ga [29,30], Sn [31] and Al [32–34]. The substitutions aim to lower T_C and T_{str}, thus creating coupled structural and magnetic transitions at RT.

In this article, we investigate a series of MM'X compositions with abundant elements, featuring the least expensive MM'X possible: $Mn_{1-x}Ni_{1-x}Fe_{2x}Si_{0.95}Al_{0.05}$ with x = 0.28, 0.3, 0.32 and 0.35. All reports so far have dealt with single site substitutions. To the best of our knowledge, no concurrent Al (2*c*) substitutions with double (2*a*, 2*d*) site substitutions by Fe have been reported.

The structures, phase content, and morphology are described by the help of powder X-ray diffraction and microscopy techniques. In addition, a comprehensive analysis of structural transitions, magnetic and magnetostructural properties are presented. This enables a fundamental understanding of the $MnNiSi_{0.95}$ $Al_{0.05}$ intermetallic with double substitution of 2*a* and 2*d* sites by Fe featuring transitions across RT.

2. Materials and methods

MnNiSi-based intermetallics were synthesized with pre-alloyed MnNiSi intermetallic ingots together with elemental Fe, Si and Al in a Ti-gettered arc melting furnace. MnNiSi pre-alloys were utilized instead of the pure elements as the samples featured a smaller mass loss. Mass losses due to Mn evaporation were smaller than 1 wt% in all samples. The as-cast ingots were subsequently sealed in quartz tubes under vacuum, heat treated at 1073 K for 7 days and quenched in water.

Synchrotron radiation powder X-ray diffraction (SR-PXD) experiments were carried out at the Swiss-Norwegian Beamline (SNBL), station BM-01, ($\lambda = 0.69217$ Å) at the European Synchrotron Radiation Facility (ESRF) in Grenoble, France. Heating and cooling of the capillaries was performed using a cryostat or a furnace with heating/cooling rates of 2K/min. Structural characterization was performed in Topas Academic v6. In all refinements, the peak resolution function was described by an algorithm developed by Chernyshov et al. [35] for area detectors, such as the one at BM-01. The background was described by a Chebyschev polynomial with 10 parameters. The main parameters refined were zero error, lattice parameters, general positions and isotropic displacement factors for individual sites. Size broadening of the peaks was described using a Lorentzian function. Preferential Orientation was addressed by the use of the March-Dollase model whose pole density profile is given by

$$P_{p*}(r,\rho) = \left(r^3 \cos^2\rho + \frac{\sin^2\rho}{r}\right)^{-3/2} \quad (1)$$

Where p* represents the preferred orientation direction, defined as p* = ha* + kb* + lc* for the reciprocal lattice vectors a*, b* and c*, and r is a parameter for description of crystallites impacting the preferred orientation, where values smaller than 1 describe rod-shaped crystallites, and r larger than 1 describe plate-shaped crystallites. The angle ρ is the polar angle between the preferred orientation direction p* and the direction s*

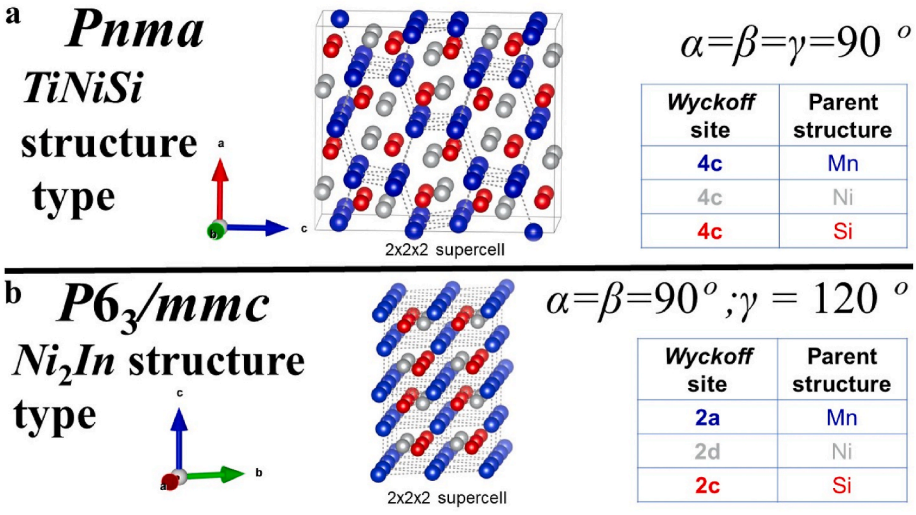

Fig. 1. Representation of the structure and description of the main parameters of the orth. and hex. structures adopted in MnNiSi compounds.

that specifies the direction of the specimen [36].

Optical micrographs were obtained from a Zeiss Axioskop 2 with a polarizer lens. Scanning electron microscopy (SEM) and energy dispersive X-ray spectroscopy (EDS) were done in a Hitachi SU8230 ultra-high resolution cold-field emission scanning electron microscope.

Differential scanning calorimetry (DSC) measurements were carried out with a Discovery DSC 25 from TA Instruments using a heating/cooling rate of 10 K/min in ingots with masses in the range of 5–15 mg. Heat capacity measurements were performed by a "classical" three step procedure [37]. Magnetic measurements were performed by a Quantum Design MPMS 3, where temperature dependent curves had applied fields of $\mu_0 H = 0.5$ T, and heating rates of 2 K/min from 50 to 375 K. Field dependent curves were performed by the discontinuous method [38] with temperature intervals of 2 K/min in magnetic fields in the range of $\mu_0 H = 0$–7 T across the magnetic transitions. The samples had masses ranging from 20 to 40 mg and were not corrected for demagnetization.

3. Results and discussion

3.1. Crystal structure and microstructure

The SR-PXD patterns at RT presented in Fig. 2 show the presence of both orth. and hex. phases for all compositions. The partial Fe substitution in both Mn and Ni sites acts to stabilize the hex. *Ni_2In* structure type at RT. This is confirmed by the gradual growth of all hex. peaks, but most notably the $(102)_{hex}$, and $(110)_{hex}$ planes seen between 2 θ = 19–20°, see Fig. 2. This growth occurs in detriment of the orth. peaks. A third set of peaks, which corresponds to $Mn_{1.0}Ni_{1.25}Si_{0.75}$ in the hexagonal *$MgZn_2$* structure-type (*$P6_3/mmc$*), can be observed for all samples [39]. For the x = 0.28 sample, a small peak associated with the $(3\bar{1}0)$ reflection for the Fe_5Si_3-type hexagonal phase is present in the pattern in $2\theta = 17.87°$. Other Fe_5Si_3 peaks are overlapping with reflections from other structures.

Rietveld refinements were carried out on all X-ray patterns and are also shown in Fig. 2. The results show that the phase content at RT is modified as a function of Fe substitution, increasing the amount of hex. phase with higher Fe contents seen in Fig. 3. The main lattice parameters, standard deviations, volume of the orth. and hex. unit cells, and

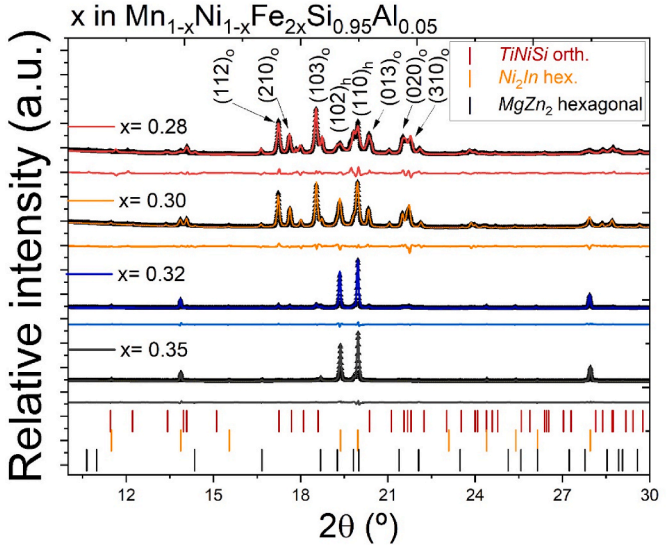

Fig. 2. Rietveld refinement results of SR-PXD data (λ = 0.69217 Å) of $Mn_{1-x}Ni_{1-x}Fe_{2x}Si_{0.95}Al_{0.05}$ with x = 0.28, 0.3, 0.32, and 0.35, displaying the main phases present at RT on the bottom of the graph, and the main miller indices of the orth. and hex. phases between 2Θ = 17–23°. Experimental data is represented by symbols, the best fit as continuous lines and the difference plot is shown under each diffraction pattern.

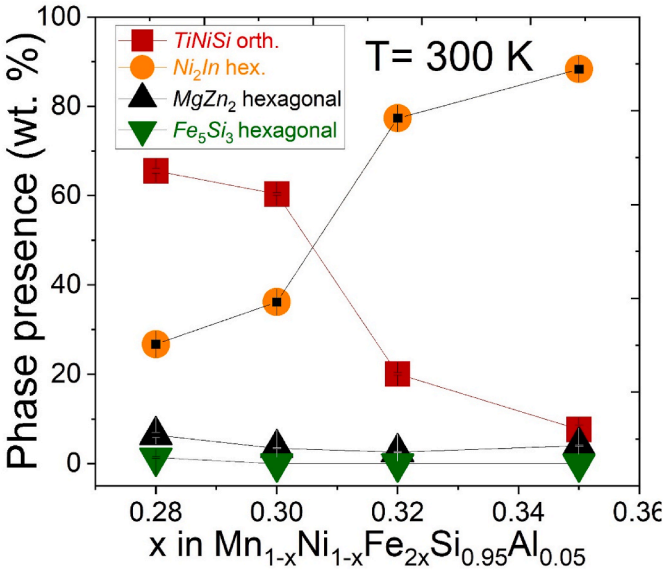

Fig. 3. Phase presence for different compositions of $Mn_{1-x}Ni_{1-x}Fe_{2x}Si_{0.95}Al_{0.05}$ as a function of Fe content as determined by Rietveld refinement.

weighted profile R-factors (R_{wp}) for all samples are displayed in Table 1. A small reduction of the unit cell volume with increasing Fe substitution can be observed for both the hex. and orth. cell.

There was a challenge to fit the observed intensities for the (102) and (110) peaks for the *Ni_2In* structure, which could be an indication of preferential orientation in the samples. A March-Dollase model was used and successfully described the intensity mismatches with (hkl) of (110), and r values ranging from 0.76 to 0.85, see eqn. (1) above. Such preferential orientation in the sample can be attributed to the solidification process. The arc melting process occurs by opening an electric arc through the sample and into a Cu coated cooled hearth. As the melting is finished, the grains quickly crystallize from the colder Cu interface, inducing columnar growth, which in turn aligns the grains. This should create a texture in the microstructure, which is confirmed by polarized optical microscopy technique, employed for the $Mn_{0.68}Ni_{0.68}Fe_{0.64}Si_{0.95}Al_{0.05}$(x = 0.32) sample, see Fig. 4a. Polarized images are a helpful tool as different grain orientations can be differentiated by different grey hues.

Fig. 4a shows that the microstructure is composed of long, slab-like grains with lengths in the order of hundreds of micrometers, following the solidification front. Higher magnifications (63x) provide a better understanding of the microstructure in Fig. 4b. The grains of the main phase appear to be surrounded by dark boundary regions. The same tone is observed in inclusions, as seen within the "matrix" composed of the *Ni_2In* hex. phase.

These inclusions and dark boundary areas could be an indication of a secondary phase. Using SEM imaging and EDS measurements, this suspicion can be further elucidated. Indeed, the presence of a chemically different phase in the grain boundaries is confirmed by SEM measurements in Back-scattered electron mode, see Fig. 4c. This is because different atomic densities are observed between the "matrix phase" and the secondary phase, indicating different elemental compositions. This secondary phase is present in the grain boundaries of the *NiIn* structure and inside the grains. With the aid of composition maps, shown in Fig. 4d, one can clearly note a lower presence of Fe in the secondary phase and a higher presence of Mn and Ni (not shown for the sake of brevity). EDS measurements determined the chemical composition of the secondary phase as $Mn_{0.97}Ni_{0.97}Fe_{0.28}Si_{0.78}$. This is very similar to the nominal composition of the hexagonal *$MgZn_2$* phase ($Mn_{1.0}Ni_{1.25}Si_{0.75}$), with a small amount of Fe substitution that was also observed by SR-PXD (see Figs. 2 and 3).

Table 1
Structural parameters of the studied samples obtained by Rietveld refinement: lattice parameters, volume of the orth. and hex. unit cells, and weighted profile R-factors (R_{wp}) with standard deviations in brackets.

Composition $Mn_{1-x}Ni_{1-x}Fe_{2x}$ $Si_{0.95}Al_{0.05}$	a *orth* (Å)	b *orth* (Å)	c *orth* (Å)	V_{orth} (Å^3)	a *hex* (Å)	C *hex* (Å)	V_{hex} (Å^3)	R_{wp} (%)
x=0.28	5.7452(4)	3.6643(2)	6.958(5)	146.41(2)	3.9997(4)	5.1200(8)	70.93(2)	8.29
x=0.30	5.7302(3)	3.6713(2)	6.9576(3)	145.34(1)	3.9958(1)	5.1275(2)	70.901(6)	5.52
x=0.32	5.7367(4)	3.668(2)	6.950(5)	146.27(1)	3.9935(5)	5.1299(7)	70.852(2)	7.45
x=0.35	5.693(4)	3.677(2)	6.952(4)	145.1(2)	3.9913(5)	5.1200(7)	70.640(2)	8.02

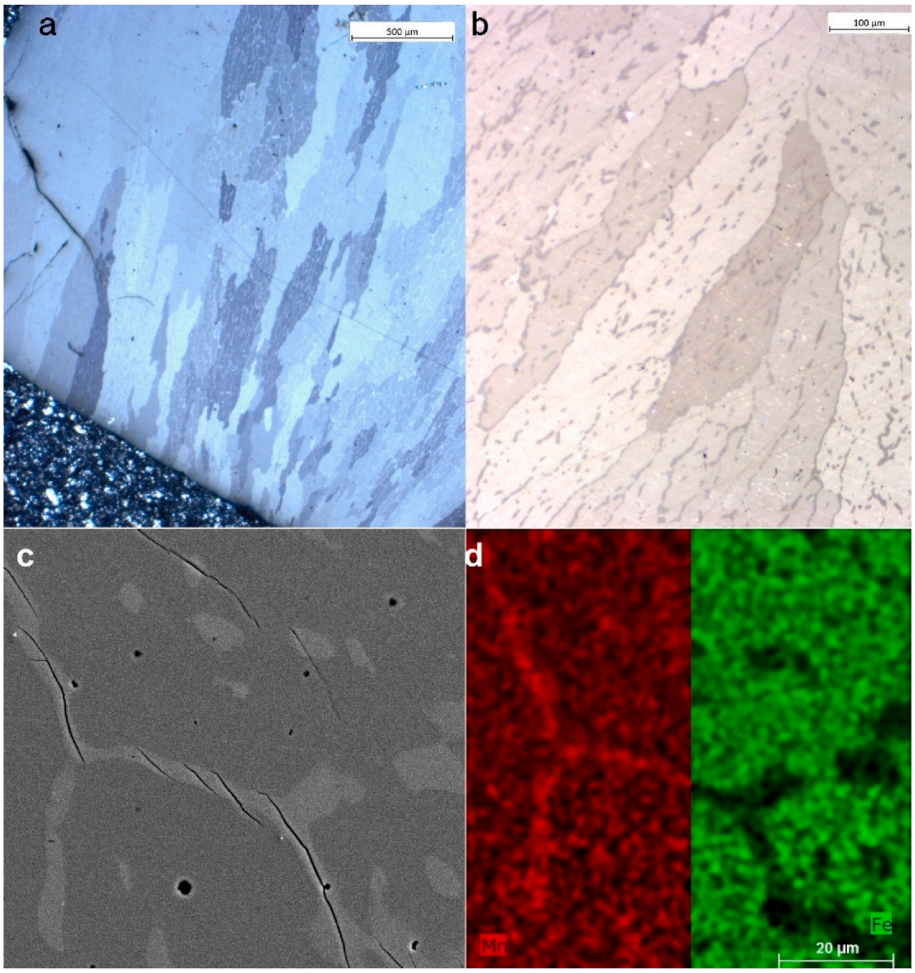

Fig. 4. Microstructure of the $Mn_{0.68}Ni_{0.68}Fe_{0.64}Si_{0.95}Al_{0.05}$ heat treated sample observed by a) polarized optical microscopy with a 16x magnification exhibiting elongated grains due to preferential orientation; b) Higher (63x) magnification which displays the biphasic nature of the sample; c) Back-scattered electron image which shows the different atomic densities, confirming the biphasic nature of the microstructure and d) Mn/Fe EDS maps of the same area, confirming the presence of a Mn-rich, Fe-poor phase – the composition traces it back to the MnNiFeSi phase with a hexagonal $MgZn_2$-type structure.

The presence of such $MgZn_2$ Laves structure can be rationalized by the following reasons: Firstly, in the MnNiSi parent compound, the stabilization of the hex. structure at RT can only be performed by the presence of (at least) two substitutions to the lattice. In the case of Al substitution in the Si sites, the required amounts for stabilization are small, close to 1 wt %. As such, small inhomogeneities in the Al or Fe contents around the grains could stabilize the $MgZn_2$ Laves phase in the grain boundary or inside the grain regions. Secondly, the thermodynamic equilibrium of the proposed composition is inside a biphasic field. A third possibility is that the $MgZn_2$ Laves phase is segregated upon solidification and not solubilized during heat treatment. Additional EDS measurements on a series of areas encompassing the dark and bright phases were carried out, thereby determining the composition of the alloy, to be $Mn_{0.7}Ni_{0.67}Fe_{0.67}Si_{0.90}Al_{0.06}$, and thus in good agreement with the nominal composition $Mn_{0.68}Ni_{0.68}Fe_{0.64}Si_{0.95}Al_{0.05}$.

3.2. Structural transitions characterized by SR-PXD and DSC

In-situ SR-PXD is a powerful technique to study structural transitions as a function of temperature. An example of the transition in $Mn_{0.7}Ni_{0.7}Fe_{0.6}Si_{0.95}Al_{0.05}$ is shown in Fig. 5 during heating with a heating rate of 2 K per minute. In this contour plot, the peaks associated with the orth. phase are disappearing with increasing temperature while the hex. peaks are becoming stronger in intensity. Small peaks associated with the $MgZn_2$ structure-type can also be observed in the vicinity of the peaks from the Ni_2In structure-type. The reduction and gradual disappearance of the orth. peaks occur between 320 and 380 K, respectively. This large temperature range could be an indication of the level of disorder associated with the structure, as Mn/Fe/Ni can interchangeably occupy 2*a* and 2*d* sites, respectively. This can also be a reason for the presence of hex. peaks at lower temperatures, before the majority of the sample undergoes the phase transition. By analysing the derivative of the intensity of the $(110)_{hex}$ peak with temperature, one can observe the temperature regions where the transition takes place.

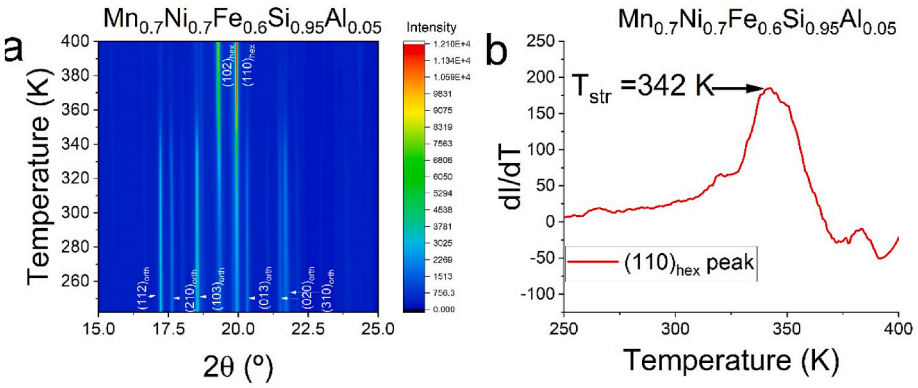

Fig. 5. a) Contour plot for the diffraction patterns as a function of temperature for $Mn_{0.7}Ni_{0.7}Fe_{0.6}Si_{0.95}Al_{0.05}$. ($\lambda = 0.69217$ Å) The plot displays the transition from the orth. to hex. structure occurring across the measured temperatures. b) derivative of intensity as a function of temperature for the $(110)_{hex}$ peak, indicating the transition temperature occurring in the measured composition.

The T_{str} is found to be around 342 K in Fig. 5b.

An alternative method to characterize structural transitions in a material is by capturing the latent heat associated with such transitions in a DSC device. By modification of the Fe content in $Mn_{1-x}Ni_{1-x}Fe_{2x}Si_{0.95}Al_{0.05}$, the transition temperatures between orth. and hex. structures changes from above to significantly below RT by decreasing x, see the DSC curves in Fig. 6a. Transition temperatures for orth. to hex. structure ($Tstr_{orth-hex}$) during heating, hex. to orth. ($Tstr_{hex-orth}$) during cooling, and thermal hysteresis values are displayed in Table 2. Values for the transformation temperatures are obtained from the maximum/minimum value of heat flow for each sample. The samples with x = 0.28 and 0.30 feature transitions above RT, with transitions between 373 and 419 K, and 313 and 351 K, respectively. The x = 0.32 and 0.35 samples feature transitions below RT, between 226-270 K and 183–217 K, respectively. Therefore, going from x = 0.28 to x = 0.35 substantially impacts Tstr, modifying it by almost 200 K. The peaks are broad across the transitions for x = 0.32, 0.3 and 0.28, which is another indication of the local disorder in the system. For the x = 0.35 sample, a sharp transition is observed, which can be associated with a smaller disorder in the small ingot measured. Thermal hysteresis is noticeable in these measurements, which range from 46, 42, 44 and 34 K for the samples with x = 0.28, 0.30, 0.32 and 0.35, respectively. Such values are relatively high and can be attributed to extrinsic and intrinsic factors [40], but also due to the thermal inertia component, as calorimetry measurements are dynamic measuring processes, with high heating and cooling rates (10 K/min in the performed measurements).

Another method to extract information from scanning calorimetry experiments is by measuring the heat capacity of a sample, obtained through a "classical" three-step procedure, seen in the cooling transition of Fig. 7a for $Mn_{0.7}Ni_{0.7}Fe_{0.6}Si_{0.95}Al_{0.05}$. By doing this, it is possible to extract the absolute entropy variation before and after the structural transition ΔS_{str}. To determine the entropy change associated to the event, two lines are drawn from the curve before and after the transition event. By drawing a line from the inflection point of the transition and connecting it to the two aforementioned curves, the associated entropy values from initial (Ti) and final (Tf) points can be subtracted, obtaining the entropy variation before and after the transition. For the $Mn_{0.7}Ni_{0.7}Fe_{0.6}Si_{0.95}Al_{0.05}$ composition, the variation of entropy is approximately 51 J/Kg.K.

Table 2
Transition temperatures during heating and during cooling in $Mn_{1-x}Ni_{1-x}Fe_{2x}Si_{0.95}Al_{0.05}$ obtained by DSC and by temperature dependent magnetization, and T_{hys} values for the produced samples.

Composition $Mn_{1-x}Ni_{1-x}Fe_{2x}Si_{0.95}Al_{0.05}$	Transition temperature (K)		T *hys* (K)	Transition temperature (K)		T *hys* (K)
	DSC	DSC	DSC	VSM	VSM	VSM
	Heating	Cooling	T_{hys}	Heating	Cooling	T_{hys}
x= 0.28	419	373	46	–	–	–
x= 0.3	351	313	38	347	324	23
x= 0.32	270	226	44	270	240	30
x= 0.35	217	183	34	219	183	36

3.3. Magnetic and magnetocaloric properties

Temperature-dependent magnetization curves for samples with x = 0.30, 0.32 and 0.35 are shown in Fig. 6b. The sample with x = 0.28 features a transition beyond the measuring capacity of the MPMS system, and thus it has been excluded here. To capture the transitions in the

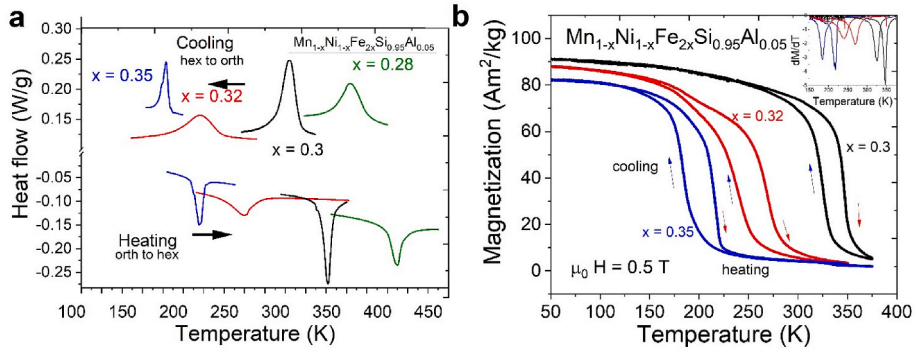

Fig. 6. The MST observed in $Mn_{1-x}Ni_{1-x}Fe_{2x}Si_{0.95}Al_{0.05}$ (x = 0.28, 0,30, 0.32 and 0.35) by means of a) DSC and b) temperature-dependent magnetization measurements.

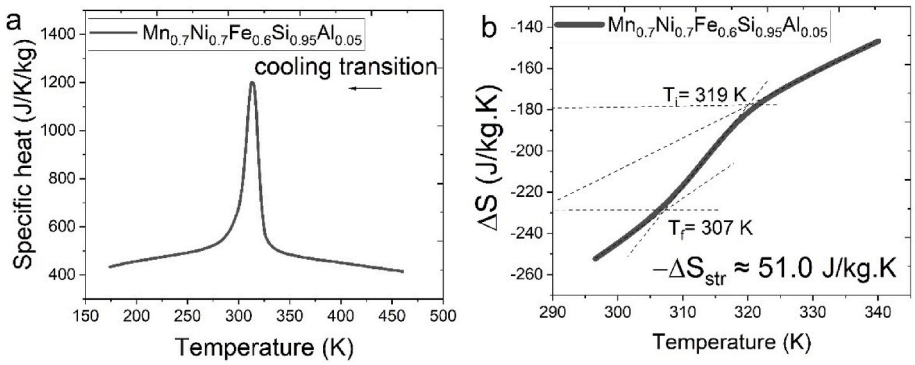

Fig. 7. a) Heat capacity obtained from DSC measurements for the cooling transition of $Mn_{0.7}Ni_{0.7}Fe_{0.6}Si_{0.95}Al_{0.05}$. b) Absolute variation in entropy for the structural transition region of the sample $Mn_{0.7}Ni_{0.7}Fe_{0.6}Si_{0.95}Al_{0.05}$, which allows for the determination of the entropy change due to the latent heat of the transition.

examined samples, applied fields of $\mu_0 H = 0.5$ T were used. With higher Fe substitution, the absolute magnetization decreases, which might seem counterintuitive. In fact, due to the interatomic distances in the lattices, the Mn atom carries a higher FM moment than Fe in the *TiNiSi* and the *Ni_2In* structures. Generally, the presence of transition metals in Mn sites impacts the magnetization by changing the average interatomic distances between Mn–Mn atoms, and through modification of the band structure. Nevertheless, Fe substitution results in the smallest decrease of magnetization [32]. The abrupt change of magnetization at temperatures close to the latent heat peaks seen in the DSC, as the samples are heated/cooled, is a clear indication of an MST. The presence of a small dip between 180 and 230 K and a wider transition in the x = 0.32 sample could be an indication of a higher degree of inhomogeneity, displaying more than a single magnetic phase undergoing a transition inside that temperature region. As the MnNiSi system features a wide solid solubility region when Fe is incorporated into the lattice, compositional variations can occur within the small amounts of mass present (between 10 and 30 mg) in the magnetization measurements. Nevertheless, the other samples appear to feature only one magnetic phase transition. Another interesting feature of the martensitic transformation in such compositions is the difference in transition temperature width between heating and cooling steps, indicating different mechanisms for each event. During the heating transformation, an anisotropic contraction of the cell volume is observed, inducing tensile residual stress. On the cooling transformation, the stress is released by the expansion, and by the formation of new surface area i.e., cracking of the sample.

The magnetic transition temperatures measured by magnetometry are displayed in Table 2. Temperatures obtained by VSM during cooling are 324, 240 and 183 K, and 347, 270 K and 219 K during heating, for x = 0.3, 0.32, and 0.35, respectively. The transitions measured by magnetometry feature smaller hysteresis than those obtained by DSC measurements, with 23 and 30 K for x = 30 and x = 0.32, respectively. This is due to the fact that the magnetic measurements were performed with a lower heating/cooling rate of 2 K/min, instead of 10 K/min used in the DSC. Further analysis of the magnetocaloric properties requires the use of field dependent curves, which allow the determination of the isothermal entropy change. As the x = 0.3 sample is the one that features most of its transition close to RT, we analyse its cooling transition in detail.

3.4. *Magnetocaloric effect of $Mn_{0.7}Ni_{0.7}Fe_{0.6}Si_{0.95}Al_{0.05}$*

In order to avoid the presence of mixed magnetic states during the measurements [38], the sample was always heated up to temperatures far above $Tstr_{orth\text{-}hex}$ and cooled down to the isotherm temperature without any applied field. By this method, magnetization isotherms were obtained from 310 to 364 K with a temperature step of 2 K, and are displayed in Fig. 8a to describe the cooling transformation.

The isotherms describe FM behavior at initial temperatures, with saturation magnetization reaching up to 80 Am^2/kg. As the temperature increase, a higher fraction of sample becomes PM, which leads to a decrease in magnetization. As magnetic fields increase, however, magnetization rises again after a certain applied field threshold, signaling the transition from the hex. (PM) to the orth. (FM) phase. This behavior can be seen up to 344 K, when the transformation can no longer be induced by the applied fields. When comparing the behavior with other MM'X compounds such as MnCoGe or La–Fe–Si based materials, we find that much higher fields are necessary to fully transform the material [7,22]. By employing the Maxwell relation, ΔS_m is obtained and displayed in Fig. 8b. Calculated values of ΔS_m are −8.15, −19.15 and −26.45 J/kg.K for $\mu_0 H$ = 0–2, 0–5 and 0–7 T, respectively. The negative values are an indication of conventional magnetocaloric effect.

The metamagnetic transition (PM-to-FM) seen during isotherms, the shift of ΔS_m towards higher temperatures as higher fields are applied, and the presence of hysteresis are clear indications of a FOPT. However, ΔS_m increases linearly with applied field, as shown in Fig. 8c, which is

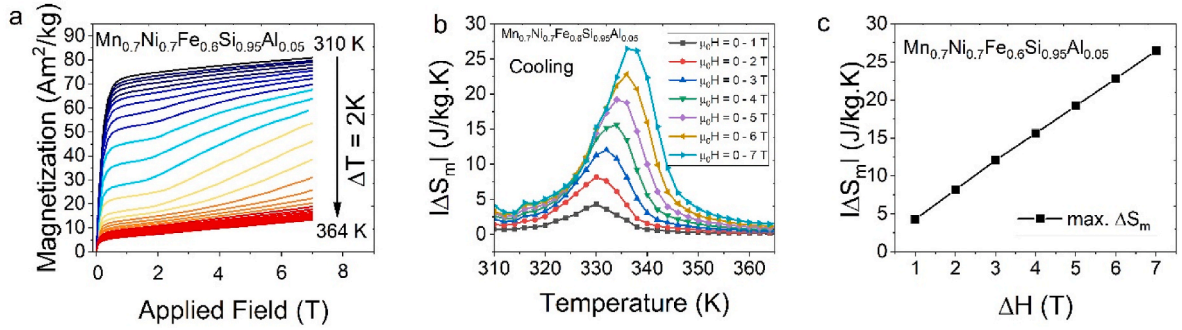

Fig. 8. Magnetic analyses for the $Mn_{0.7}Ni_{0.7}Fe_{0.6}Si_{0.95}Al_{0.05}$ sample. a) Field dependent curves across the MST, with temperature steps of 2K. b) Calculated isothermal entropy (ΔSm) in magnetic fields up to 7 T. c) Maximum variation of ΔS_m as a function of applied field, showing a linear trend.

characteristic for materials undergoing a second order phase transition [4,41]. This occurs as the maximum applied field is apparently not high enough to fully transform the material from the PM to the FM state, as can be seen from Fig. 8a. Across the temperatures where metamagnetic transitions occur, the magnetization curve does not saturate, and only reaches a fraction of the saturation magnetization seen at lower temperatures. Therefore, as higher fields transform bigger volume fractions of the sample to the FM state, the entropy change contribution associated to the martensitic transformation is higher, thus yielding a linear correlation. Assuming that the value of $|\Delta S_m|$ is the sum of the magnetic entropy due to magnetic moment reorientation ΔS_{mag}, and the fraction of the structural transition contribution ΔS_{str} due to the magnetization, one can conclude that even with applied fields of $\mu_0 H = 0$–7 T, the total $|\Delta S_m|$ is smaller than $|\Delta S_{str}|$, an indication of a low magnetostructural coupling of the studied sample.

To further investigate this MST, an Arrott plot analysis (M^2 (H/M) curves) was performed and the result is shown in Fig. 9a. Typically, an S-shaped curve or a negative slope in such plots are a qualitative indication of FOPTs [42]. A slight negative slope can be observed at T = 338 K, indicating a FOPT character. Such analysis can be useful for a qualitative evaluation of the transitions. A more sensitive method that yields a quantitative analysis has been utilized by Law et al. when studying the n exponent from the field dependence of the magnetic entropy change [41,43]. The n exponent can be calculated as follows:

$$n = \frac{d\ln(\Delta S_m)}{d\ln(\Delta H)}$$

Values of n above 2 are exhibited for compounds undergoing FOPTs. From the *n* analysis of the $Mn_{0.7}Ni_{0.7}Fe_{0.6}Si_{0.95}Al_{0.05}$ sample (Fig. 9b), n is higher than 2 only in fields above 3 T. This is another indication of the low magnetostructural coupling of the samples to the MST. The shift of T with the ΔS peak with field is also only observed when the applied field is above 3 T (see also Fig. 8b). When comparing the ΔS_m values of $Mn_{0.7}Ni_{0.7}Fe_{0.6}Si_{0.95}Al_{0.05}$ with other reported quantities in the literature, they are similar to compositions with substitutions in the Mn (2*a*) sites, in (MnFe)$NiSi_{1-y}Al_y$ [32,34,44,45]; and higher than the reported compositions with a substitution on Ni (2*d*) sites Mn(FeNi)Si_{1-y} Al_y [33]. For the $Mn_{1-x}Fe_{1-x}NiSi_1Al_{1-y}$ samples, very different values are reported for similar compositions with Fe substitution on Mn. ΔS_m values of 20–50 J/kg.K in $\mu_0 H = 0$–5 T, or between $\Delta S_m = -8$ to -22 J/kg.K in $\mu_0 H = 0$–2 T are reported, for variations of 10% of Fe substitution in Mn, or 3–4% substitution in Al [20,32]. A possible reason for the variation in values are different processing conditions such as arc-melting or melt-spinning, which modifies the structure/microstructure. Another possible reason for the variations reported in literature is how the magnetic measurements have been performed, as different starting materials placed in the magnetometer (i.e. ingots/coarse powders/fine powders) are known to modify the MSTs [46].

These variations on reported values of ΔS_m in $Mn_{1-x}Fe_{1-x}NiSi_1Al_{1-y}$ shed light on how sensitive the MST of (MnFe)Ni(SiAl) and (MnFe)(NiFe)(SiAl) compounds can be to different processing conditions that will impact ΔS_m values. Pertaining extrinsic factors, the presence of phase impurities would change the susceptibilities and magnetization of the orth. phase. In the presently studied $Mn_{1-x}Ni_{1-x}Fe_{2x}Si_{0.95}Al_{0.05}$ compositions, the secondary $Mn_{0.97}Ni_{0.97}Fe_{0.28}Si_{0.78}$ phase with a hexagonal *MgZn*2 structure is known to display antiferromagnetic (AFM) ordering [39]. This could interfere with the internal magnetization of the main hex. phase by lowering the total magnetization of the system. Therefore, removing secondary phases can help maximizing internal magnetization. To further understand this interaction between the primary and secondary magnetic phases, micromagnetic simulations could be carried out. Regarding intrinsic properties, the degree of chemical disorder in the phases is also a factor that contributes to diminished ΔS_m values, as Mn/Fe/Ni can theoretically substitute 2*a* and 2*d* sites interchangeably [32,33], while Al could substitute 2*a* and 2*c* sites [32]. This could result in a small distribution of T_{str}'s, which in turn requires a higher applied field to induce the transformation, and thus lead to a decrease in overall ΔS_m values [47]. The broad transition captured by in-situ SR-PXD as well as by DSC measurements also hint towards a distribution of T_{str}'s as a result of chemical disorder. However, such disorder can only be probed at the local level by techniques such as total scattering or X-ray absorption spectroscopy which is outside the scope of this work.

Another concern is the known effect of Mn loss during arc melting (the most reported technique for synthesis of MM'X compounds) and to a small extent during heat treatment (as it applies only to the surface areas), making it difficult to accurately track Mn concentrations across the sample. This is very important as very small variations in Mn content have a huge impact on T_{str}, altering it by 80 K for variations of 0.03 per formula unit [24]. A better microstructural design and composition control could lead to improved magnetostructural coupling and therefore higher magnetocaloric effect under lower fields. A suggestion would be to employ different synthesis and processing techniques e.g., reactive/fast sintering methods, avoiding Mn loss issues coupled with different disorder/defect concentrations.

4. Conclusion

Ingots of critical-element free $Mn_{1-x}Ni_{1-x}Fe_{2x}Si_{0.95}Al_{0.05}$ compounds (x = 0.28, 0.3, 0.32 and 0.35) were synthesized by arc-melting. The increase in Fe content lowers the cell volumes slightly and shifts magnetostructural transitions from above RT in x = 0.28 to significantly below RT in x = 0.35. The samples with x = 0.3 and 0.32 display a transition around RT.

SR-PXD at RT shows the presence of an orth. *TiNiSi*-type and a hex. Ni_2In-type phase, as well as a secondary hexagonal $MgZn_2$-type phase for all samples. Rietveld analysis evidences the presence of texture in the

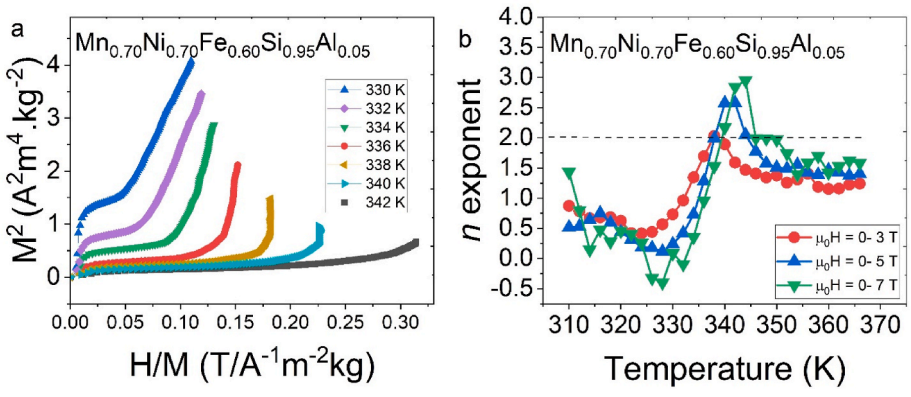

Fig. 9. Magnetic analyses for the $Mn_{0.7}Ni_{0.7}Fe_{0.6}Si_{0.95}Al_{0.05}$ sample: a) Arrott plot of the MST. b) n exponent analysis of the magnetic entropy change.

hex. *Ni_2In*-type main phase. In order to evaluate the presence of the secondary phase, and its relationship with the main phases, optical and electron microscopy techniques were applied for the sample with x = 0.32. Microscopy supports the presence of texture in the samples, which is in direct relation with formation of a solidification front during arc melting, confirming previous results from SR-PXD. The secondary *$MgZn_2$*-type phase is primarily located at the grain boundaries and to a lesser extent, is also present inside the grains of the main phase. The composition of the secondary *$MgZn_2$*-type phase obtained by EDS measurements is $Mn_{0.97}Ni_{0.97}Fe_{0.28}Si_{0.78}$.

The magnetostructural transitions are evaluated by in-situ SR-PXD, heat capacity and heat flow measurements by DSC, and magnetic measurements. Transformation temperatures for the orth.to hex. transition span a broad region from above to below RT and were determined as 419, 351, 270 and 217 K for x = 0.28, 0.30, 0.32, and 0.35, respectively. Magnetic measurements show magnetic transitions at 347, 270 and 219 for x = 0.3, 0.32 and 0.35, respectively, under an applied field of $\mu_0 H = 0.5$ T. Differences between the transformation temperatures obtained by DSC and magnetometry can be attributed to small compositional variations, different heating rates and the influence of the magnetic field.

The hex. to orth. transition i.e., cooling transformation is evaluated for the $Mn_{0.7}Ni_{0.7}Fe_{0.6}Si_{0.95}Al_{0.05}$ composition by field dependent isotherms, with temperature steps of 2 K, from 310 to 364 K. Entropy changes of $\Delta S_m = -8.15$, -19.15 and -26.45 J/kg.K are obtained for field changes of $\mu_0 H = 0$–2, 5 and 7 T, respectively. The results are comparable to other reported (MnFe)$NiSi_{1-y}Al_y$ compounds produced by arc melting and melt spinning. When comparing the results to other known MM'X systems with Fe/Al substitution, however, discrepancies are seen in the ΔS_m values, mostly due to the apparent low magnetostructural coupling of the MM'X materials seen in reported $Mn_{1-x}Fe_{1-x}NiSi_1Al_{1-y}$ alloys and in our samples, as confirmed by n exponent analysis. Such insensitivity could be caused by a combination of intrinsic or extrinsic effects. Therefore, more research on understanding and modifying the local structure is required to obtain critical-element free MM'X systems which can be competitive with other available magnetocaloric materials.

CRediT roles

Bruno G. F. Eggert: Conceptualization (equal)Data curation (equal) Formal analysis (equal) Investigation (equal) Methodology (equal) Visualization (equal) Writing - original draft (equal) Writing - review & editing (equal) **J. F. H. Belo:** Investigation (equal)Resources (equal) Writing - review & editing (equal) **J. P. Araújo:** Resources (equal) Writing - review & editing (equal) **Bjørn Hauback:** Supervision (equal) Writing - review & editing (equal) **Christoph Frommen:** Funding acquisition (equal)Project administration (equal) Supervision (equal) Writing - review & editing (equal)

Declaration of competing interest

The authors declare that they have no known competing financial interests or personal relationships that could have appeared to influence the work reported in this paper.

Data availability

Data will be made available on request.

Acknowledgements

This work was financed by The Research Council of Norway through the NANO2021 program, Project No. 287150. J. H. Belo thanks projects financed by EEA grants, via the project FBR OC1 85 and the national funding agency for science, research and technology (FCT) for the projects UIDB/50011/2020, PTDC/EME-TED/3099/2020, and PTDC/FISMAC/31302/2017. J. H. Belo also thanksCERN/FISTEC/0003/2019 and for his contract DL57/2016 reference SFRH-BPD-87430/2012. The authors thank the staff at the Swiss-Norwegian beamline (BM01) of the European Synchrotron Radiation Facility (ESRF) for their skillful assistance during the X-ray diffraction measurements.

References

[1] C.L. Zhang, Y.X. Zheng, H.C. Xuan, S.C. Ma, Q.Q. Cao, D.H. Wang, Y.W. Du, Large and highly reversible magnetic field-induced strains in textured Co1-xNixMnSi alloys at room temperature, J. Phys. D Appl. Phys. 44 (2011), https://doi.org/10.1088/0022-3727/44/13/135003.

[2] Q. Zhang, W.F. Li, N.K. Sun, J. Du, Y.B. Li, D. Li, Y.Q. Zhang, Z.D. Zhang, Large magnetoresistance over an entire region from 5 to 380 K in double helical CoMnSi compound, J. Phys. D Appl. Phys. 41 (2008), https://doi.org/10.1088/0022-3727/41/12/125001.

[3] C. Biswas, R. Rawat, S.R. Barman, Large negative magnetoresistance in a ferromagnetic shape memory alloy: Ni2+x Mn1-x Ga, Appl. Phys. Lett. 86 (2005) 1–3, https://doi.org/10.1063/1.1925757.

[4] A. Smith, C.R.H. Bahl, R. Bjørk, K. Engelbrecht, K.K. Nielsen, N. Pryds, Materials challenges for high performance magnetocaloric refrigeration devices, Adv. Energy Mater. 2 (2012) 1288–1318, https://doi.org/10.1002/aenm.201200167.

[5] J.S. Kouvel, C.C. Hartelius, Anomalous magnetic moments and transformations in the ordered alloy FeRh, J. Appl. Phys. 33 (1962) 1343–1344, https://doi.org/10.1063/1.1728721.

[6] A. Chirkova, K.P. Skokov, L. Schultz, N.V. Baranov, O. Gutfleisch, T.G. Woodcock, Giant adiabatic temperature change in FeRh alloys evidenced by direct measurements under cyclic conditions, Acta Mater. 106 (2016) 15–21, https://doi.org/10.1016/j.actamat.2015.11.054.

[7] J. Liu, J.D. Moore, K.P. Skokov, M. Krautz, K. Löwe, A. Barcza, M. Katter, O. Gutfleisch, Exploring La(Fe,Si)13-based magnetic refrigerants towards application, Scripta Mater. 67 (2012) 584–589, https://doi.org/10.1016/j.scriptamat.2012.05.039.

[8] Y. Liu, X. Fu, Q. Yu, M. Zhang, J. Liu, Significant reduction of phase-transition hysteresis for magnetocaloric (La1-xCex)2Fe11Si2Hy alloys by microstructural manipulation, Acta Mater. 207 (2021), https://doi.org/10.1016/j.actamat.2021.116687.

[9] V.K. Pecharsky, K. a Gschneidner, Giant magnetocaloric effect in Gd 5 Si 2 Ge 2, Phys. Rev. Lett. 78 (1997) 3–6, https://doi.org/10.1103/PhysRevLett.78.4494.

[10] A. Planes, L. Mãosa, M. Acet, Magnetocaloric effect and its relation to shape-memory properties in ferromagnetic Heusler alloys, J. Phys. Condens. Matter 21 (2009), https://doi.org/10.1088/0953-8984/21/23/233201.

[11] J. Liu, T. Gottschall, K.P. Skokov, J.D. Moore, O. Gutfleisch, Giant magnetocaloric effect driven by structural transitions, Nat. Mater. 11 (2012) 620–626, https://doi.org/10.1038/nmat3334.

[12] T. Gottschall, K.P. Skokov, M. Fries, A. Taubel, I. Radulov, F. Scheibel, D. Benke, S. Riegg, O. Gutfleisch, Making a cool choice: the materials library of magnetic refrigeration, Adv. Energy Mater. 9 (2019), https://doi.org/10.1002/aenm.201901322.

[13] H. Johra, K. Filonenko, P. Heiselberg, C. Veje, S. Dall'Olio, K. Engelbrecht, C. Bahl, Integration of a magnetocaloric heat pump in an energy flexible residential building, Renew. Energy 136 (2019) 115–126, https://doi.org/10.1016/j.renene.2018.12.102.

[14] R. Gauß, G. Homm, O. Gutfleisch, The resource basis of magnetic refrigeration, J. Ind. Ecol. 21 (2017) 1291–1300, https://doi.org/10.1111/jiec.12488.

[15] T.E. Graedel, R. Barr, C. Chandler, T. Chase, J. Choi, L. Christoffersen, E. Friedlander, C. Henly, C. Jun, N.T. Nassar, D. Schechner, S. Warren, M.Y. Yang, C. Zhu, Methodology of metal criticality determination, Environ. Sci. Technol. 46 (2012) 1063–1070, https://doi.org/10.1021/es203534z.

[16] C.J. Müller, On Evil Twins and Their Absent Friends Ternary Intermetallic Ni 2 in Type, 2015.

[17] G.A. Landrum, R. Hoffmann, J. Evers, H. Boysen, The TiNiSi family of compounds: structure and bonding, Inorg. Chem. 37 (1998) 5754–5763, https://doi.org/10.1021/ic980223e.

[18] F.R. Shen, F.X. Hu, Z.B. Yu, H.B. Zhou, H. Wu, Q.Z. Huang, J.Z. Hao, Y.H. Gao, K. M. Qiao, J. Li, C. Zhang, W.H. Liang, L.H. He, J. Wang, T.J. Liang, J.R. Sun, B. G. Shen, Neutron diffraction study on hydrostatic pressure regulated magnetostructural transition and magnetocaloric effect in MnNi1 - XFexSi1 - yGey alloys, J. Appl. Phys. 127 (2020), https://doi.org/10.1063/5.0003056.

[19] W. Bażela, A. Szytula, J. Todorović, A. Zięba, Crystal and magnetic structure of the NiMnGe 1− nSin System, Phys. Status Solidi 64 (1981) 367–378, https://doi.org/10.1002/pssa.2210640140.

[20] C.L. Zhang, H.F. Shi, Y.G. Nie, E.J. Ye, Z.D. Han, D.H. Wang, Thermal-cycling-dependent magnetostructural transitions in a Ge-free system Mn0.5Fe0.5Ni(Si,Al), Appl. Phys. Lett. 105 (2014), https://doi.org/10.1063/1.4904464, 0–4.

[21] S.C. Ma, Y.X. Zheng, H.C. Xuan, L.J. Shen, Q.Q. Cao, D.H. Wang, Z.C. Zhong, Y. W. Du, Large roomtemperature magnetocaloric effect with negligible magnetic hysteresis losses in Mn1-xVxCoGe alloys, J. Magn. Magn Mater. 324 (2012) 135–139, https://doi.org/10.1016/j.jmmm.2011.07.047.

[22] S.K. Pal, C. Frommen, S. Kumar, B.C. Hauback, H. Fjellvåg, G. Helgesen, Enhancing giant magnetocaloric effect near room temperature by inducing magnetostructural

coupling in Cu-doped MnCoGe, Mater. Des. 195 (2020), 109036, https://doi.org/10.1016/j.matdes.2020.109036.
[23] A. Taubel, T. Gottschall, M. Fries, T. Faske, K.P. Skokov, O. Gutfleisch, Influence of magnetic field, chemical pressure and hydrostatic pressure on the structural and magnetocaloric properties of the Mn-Ni-Ge system, J. Phys. D Appl. Phys. 50 (2017), https://doi.org/10.1088/1361-6463/aa8e89.
[24] E.K. Liu, W. Zhu, L. Feng, J.L. Chen, W.H. Wang, G.H. Wu, H.Y. Liu, F.B. Meng, H. Z. Luo, Y.X. Li, Vacancy-tuned paramagnetic/ferromagnetic martensitic transformation in Mn-poor Mn1-xCoGe alloys, EPL 91 (2010), https://doi.org/10.1209/0295-5075/91/17003, 0–5.
[25] S.K. Pal, C. Frommen, S. Kumar, B.C. Hauback, H. Fjellvåg, T.G. Woodcock, K. Nielsch, G. Helgesen, Comparative phase transformation and magnetocaloric effect study of Co and Mn substitution by Cu in MnCoGe compounds, J. Alloys Compd. 775 (2019) 22–29, https://doi.org/10.1016/j.jallcom.2018.10.040.
[26] C.L. Zhang, H.F. Shi, E.J. Ye, Y.G. Nie, Z.D. Han, B. Qian, D.H. Wang, Magnetostructural transition and magnetocaloric effect in MnNiSi-Fe2Ge system, Appl. Phys. Lett. 107 (2015) 2–6, https://doi.org/10.1063/1.4936610.
[27] L.M. Moreno-Ramírez, Díaz-García, J.Y. Law, A.K. Giri, V. Franco, Hysteresis, latent heat and cycling effects on the magnetocaloric response of (NiMnSi)0.66 (Fe2Ge)0.34 alloy, Intermetallics 131 (2021), https://doi.org/10.1016/j.intermet.2020.107083.
[28] E. Palacios, R. Burriel, C.L. Zhang, Calorimetric study of the giant magnetocaloric effect in (MnNiSi)0.56(FeNiGe)0.44, Phys. Rev. B 103 (2021) 1–8, https://doi.org/10.1103/PhysRevB.103.104402.
[29] C.L. Zhang, Y.G. Nie, H.F. Shi, E.J. Ye, J.Q. Zhao, Z.D. Han, H.C. Xuan, D.H. Wang, Tunable magnetostructural coupling and large magnetocaloric effect in Mn1−xNi1−xFe2xSi1−xGax, J. Magn. Magn Mater. 432 (2017) 527–531, https://doi.org/10.1016/j.jmmm.2017.02.046.
[30] H. Imam, H.G. Zhang, J. Chen, M. Yue, Q.M. Lu, D.T. Zhang, W.Q. Liu, Powdering and SPS sintering effect on the magnetocaloric properties of MnNiSi-based compounds, AIP Adv. 9 (2019), https://doi.org/10.1063/1.5070084, 0–4.
[31] K. Deepak, R.V. Ramanujan, Magnetocaloric properties of low-cost fe and sn substituted mnnisi-based alloys exhibiting a magnetostructural transition near room temperature, IEEE Trans. Magn. 54 (2018), https://doi.org/10.1109/TMAG.2018.2832090.
[32] A. Biswas, A.K. Pathak, N.A. Zarkevich, X. Liu, Y. Mudryk, V. Balema, D. D. Johnson, V.K. Pecharsky, Designed materials with the giant magnetocaloric effect near room temperature, Acta Mater. 180 (2019) 341–348, https://doi.org/10.1016/j.actamat.2019.09.023.
[33] B. Nuendute, W. Hanggai, H. Yibole, B. Tana, O. Tegus, F. Guillou, Drastic influence of synthesis conditions on structural, magnetic, and magnetocaloric properties of Mn(Fe,Ni)(Si,Al) compounds, Crystals 12 (2022), https://doi.org/10.3390/cryst12020233.
[34] L. Lei, Z.G. Zheng, S. Jin, W.H. Wang, C.F. Li, J.Y. Liu, Z.G. Qiu, D.C. Zeng, The magnetostructural transition and magnetocaloric properties in Fe0.6Mn0.4NiSi1-xAl xalloys, J. Appl. Phys. 128 (2020), https://doi.org/10.1063/5.0003261, 0–9.
[35] D. Chernyshov, V. Dyadkin, H. Emerich, G. Valkovskiy, C.J. McMonagle, W. van Beek, On the resolution function for powder diffraction with area detectors, Acta Crystallogr. Sect. A Found. Adv. 77 (2021) 497–505, https://doi.org/10.1107/s2053273321007506.
[36] T. Ida, in: Effect of Preferred Orientation in Synchrotron X-ray Powder Diffraction, 2, 2013, pp. 7–11. http://www.crl.nitech.ac.jp/ar/2013/0711_acrc_ar2013_review.pdf.
[37] G.W.H. Höhne, W. Hemminger, H.-J. Flammersheim, Differential Scanning Calorimetry, Springer Berlin Heidelberg, 1996, https://doi.org/10.1007/978-3-662-03302-9.
[38] L. Caron, Z.Q. Ou, T.T. Nguyen, D.T. Cam Thanh, O. Tegus, E. Brück, On the determination of the magnetic entropy change in materials with first-order transitions, J. Magn. Magn Mater. 321 (2009) 3559–3566, https://doi.org/10.1016/j.jmmm.2009.06.086.
[39] X. Yan, M.W. Pieper, H. Michor, G. Hilscher, M. Reissner, A. Grytsiv, P. Rogl, V. Pomjakushin, G. Giester, E. Bauer, S. Paschen, Phase relations, crystal chemistry, and physical properties of MgZn 2-type Laves phases in the Mn-Cu-Si and Mn-Ni-Si systems, Phys. Rev. B Condens. Matter 88 (2013) 1–13, https://doi.org/10.1103/PhysRevB.88.174416.
[40] O. Gutfleisch, T. Gottschall, M. Fries, D. Benke, I. Radulov, K.P. Skokov, H. Wende, M. Gruner, M. Acet, P. Entel, M. Farle, Mastering hysteresis in magnetocaloric materials, Philos. Trans. R. Soc. A Math. Phys. Eng. Sci. 374 (2016), https://doi.org/10.1098/rsta.2015.0308.
[41] V. Franco, J.S. Blázquez, A. Conde, Field dependence of the magnetocaloric effect in materials with a second order phase transition: a master curve for the magnetic entropy change, Appl. Phys. Lett. 89 (2006) 1–4, https://doi.org/10.1063/1.2399361.
[42] B.K. Banerjee, On a generalised approach to first and second order magnetic transitions, Phys. Lett. 12 (1964) 16–17, https://doi.org/10.1016/0031-9163(64)91158-8.
[43] J.Y. Law, V. Franco, L.M. Moreno-Ramírez, A. Conde, D.Y. Karpenkov, I. Radulov, K.P. Skokov, O. Gutfleisch, A quantitative criterion for determining the order of magnetic phase transitions using the magnetocaloric effect, Nat. Commun. 9 (2018), https://doi.org/10.1038/s41467-018-05111-w.
[44] M.L. Arreguín-Hernández, C.F. Sánchez-Valdés, J.L. Sánchez Llamazares, Magnetostructural transition and magnetocaloric effect in thermally annealed Mn0.5Fe0.5NiSi0.945Al0.055 melt-spun ribbons, J. Magn. Magn Mater. 533 (2021), https://doi.org/10.1016/j.jmmm.2021.168021.
[45] S. Ghosh, P. Sen, K. Mandal, Magnetostructural transition and large magnetocaloric effect in (Mn0.6Fe0.4)NiSi1−xAlx (x = 0.06–0.08) alloys, J. Magn. Magn Mater. 500 (2020) 23–26, https://doi.org/10.1016/j.jmmm.2019.166345.
[46] T. Gottschall, D. Benke, M. Fries, A. Taubel, I.A. Radulov, K.P. Skokov, O. Gutfleisch, A matter of size and stress: understanding the first-order transition in materials for solid-state refrigeration, Adv. Funct. Mater. 27 (2017) 1–6, https://doi.org/10.1002/adfm.201606735.
[47] J.S. Amaral, V.S. Amaral, Disorder effects in giant magnetocaloric materials, Phys. Status Solidi Appl. Mater. Sci. 211 (2014) 971–974, https://doi.org/10.1002/pssa.201300749.